Applied Radiation and Isotopes 156 (2020) 108975

Contents lists available at ScienceDirect

Applied Radiation and Isotopes

journal homepage: http://www.elsevier.com/locate/apradiso

Performance assessment of a 500 mm^3 CZT and a 2x2 inch $LaBr_3$(Ce) detectors for the determination of the uranium enrichment using the enrichment-meter method and calibration standards for safeguards applications

I. Meleshenkovskii [a,b], N. Pauly [b,*], P.-E. Labeau [b]

[a] Belgian Nuclear Research Centre, SCK•CEN; Environment, Health and Safety Institute, Boeretang 200, B-2400, Mol, Belgium
[b] Université libre de Bruxelles, Service de Métrologie Nucléaire (CP/165/84), 1050, Bruxelles, Belgium

ARTICLE INFO

Keywords:
CdZnTe
$LaBr_3$(Ce)
Room temperature
Uranium enrichment
Enrichment-meter
Safeguards

ABSTRACT

Determination of the uranium enrichment is an important safeguards verification task, routinely carried out using non-destructive assay methods. The enrichment-meter method is one of the most widely used passive non-destructive X- and gamma-ray based methods used for such tasks. Among its advantages is the highly constrained physical nature of its underlying formalism, allowing it to be used with high-resolution HPGe detectors, as well as with low-resolution NaI detectors. Due to attractive features and spectroscopic performance, CdZnTe and $LaBr_3$(Ce) detectors raised interest in their application to such tasks as well. However, their spectroscopic performance is different to that of the traditional detectors in many ways. Application of the enrichment-meter method requires determination of the net peak areas corresponding to ^{235}U signature photopeaks. The latter requires an adequate algorithm to select the region-of-interest boundaries, which may be sensitive to asymmetrical photopeaks of CZT detectors. In this paper we conduct a performance assessment of a 500 mm^3 CZT detector of a quasi-hemispherical design and a 2×2 inch $LaBr_3$(Ce) scintillator with the enrichment-meter method using a set of certified uranium standards with enrichment degrees from 0.31% to 4.46% of ^{235}U atomic abundance. We investigate the impact of different methods used for net peak area determination, statistical quality of acquired spectra and size of region-of-interest boundaries on accuracy and uncertainty. We propose an algorithm for symmetrical/asymmetrical region-of-interest boundaries determination and make recommendations on the best combinations of the region-of-interest size and method used for the net peak area determination for each of the detectors. The underlying routines of the algorithm and analysis procedures are described in detail and results are presented.

1. Introduction

Introduction of room temperature medium resolution detectors, such as CdZnTe (CZT) and $LaBr_3$(Ce), with superior spectroscopic performance compared to such traditional room temperature detectors as NaI, has opened new possibilities in many radiation detection applications (Sullivan et al., 2008; Prosper et al., 2012). Indeed, their compact design and absence of cryogenics are an advantage in many practical applications. CZT detectors are prized for their wide energy band gap (E_g~1.6 eV) allowing their room temperature operation, coupled with their high atomic number ($Z_{max} = 52$) yields a high intrinsic efficiency of gamma absorption compared to HPGe (Takahashi and Watanabe, 2001). Besides, CZT detector technologies have rapidly evolved from simple planar designs to advanced co-planar grid and quasi-hemispherical designs, yielding energy resolution of 1.3% at 661 keV (^{137}Cs) for a 10 mm × 10 mm x 5 mm device (Ivanov and Dorogov, 1999; Arlt et al., 2000; Ivanov et al., 2014). Nowadays these detectors are commercially available in sizes up to 4000 mm^3 (Ivanov et al., 2014), making them attractive for many practical applications. $LaBr_3$(Ce) detectors have a high light output (~60000 photons/Mev), fast response (decay constant <30 ns) and show good energy resolution (~2.2% at 662 keV ^{137}Cs) (Van Loef et al., 2001; Maghraby et al., 2014; Saint-Gobain detectors leaflet 2019).

One of the fields where attractive features and spectroscopic

* Corresponding author.
E-mail address: Nicolas.Pauly@ulb.ac.be (N. Pauly).

https://doi.org/10.1016/j.apradiso.2019.108975
Received 3 June 2019; Received in revised form 24 October 2019; Accepted 4 November 2019
Available online 6 November 2019

performance of both detectors can be advantageous is nuclear safeguards. Indeed, CZT and $LaBr_3$(Ce) detectors were proposed as possible alternatives to spectrometers based on traditional HPGe and NaI detectors for isotopic determination tasks of uranium and plutonium bearing materials (Ruhter, 1998; Sullivan et al., 2008). The energy resolution of CZT and $LaBr_3$(Ce) detectors is significantly better compared to that of NaI detectors, allowing for a more detailed information available in the measured spectrum.

Determination of the uranium enrichment can be accomplished by using different methods. These methods can be divided into destructive and non-destructive methods. Technically, determination of the uranium enrichment requires means via which the information from the decaying radioisotopes can be detected and a method to interpret it. Thus, determination of the uranium enrichment can be accomplished via mass spectroscopy, alpha spectroscopy, X- and gamma-rays spectroscopy methods (Montero et al., 2004; Richter et al., 2007). Mass spectroscopy is considered by far the most accurate method, yielding the lowest combined uncertainties on the determined enrichment (Richter et al., 2007). Alpha spectroscopy is somewhat in between of the mass spectroscopy and X- and gamma-rays spectroscopy methods in terms of accuracy and uncertainty on the determined enrichment. However, mass spectroscopy is a destructive analysis method and alpha spectroscopy has serious limitations when analyzing samples behind shielding or packaging, limiting the possible safeguards applications. Thus, passive non-destructive X- and gamma-ray based methods are the preferred methods when determination of the uranium enrichment is performed "in-situ" – without moving of the analyzed sample nor opening it. The passive non-destructive X- and gamma-ray based group of methods consists of two distinctive sub-classes. One of them represents the so-called enrichment-meter method; the second one is based on the so-called isotopic ratios method (Reilly et al., 1991). The primary difference between the two is that the former requires calibration standards relative to which the enrichment of the unknown sample is determined, the other one does not. Besides, the former is limited only to uranium enrichment determination tasks, whereas the latter can be used either for uranium and plutonium isotopic composition determination tasks. Traditionally, HPGe and NaI detectors have been the detectors of choice for these tasks with a wide range of well-developed commercially available software (Gunnink et al., 1994; Sampson et al., 1996; Gunnink, 2001; Simon et al., 2008).

The energy resolution of CZT and $LaBr_3$(Ce) detectors is somewhat in between of that of HPGe and NaI. However, the spectroscopic performance of room temperature medium resolution detectors can be quite different to that of HPGe and NaI. Thus, for example CZT detectors exhibit low-energy tailing due to incomplete charge collection properties (Takahashi and Watanabe, 2001). $LaBr_3$(Ce) detectors suffer from intrinsic activity of its ^{138}La radioisotope (Quarati et al., 2012). To plan the optimal usage of these detectors in safeguards applications with different methods for uranium and plutonium isotopic composition determination tasks the impact of such particularities on the respective performance need to be studied and well understood.

Recently, in our previous work (Meleshenkovskii et al., 2018a) a performance assessment of an isotopic ratios based method for the determination of the uranium enrichment without calibration standards using a 2×2 inch $LaBr_3$(Ce) was conducted and the MCSIGMA code optimized for $LaBr_3$(Ce) detectors was developed. Results of that work indicated a promising performance of $LaBr_3$(Ce) detectors for such tasks after the necessary modifications to the analysis and spectral information extraction routines are introduced to account for the physical and statistical particularities of $LaBr_3$(Ce) measured uranium spectra. Performance assessment of a 500 mm^3 CZT detector of a quasi-hemispherical design with an isotopic ratios method for uranium enrichment determination tasks is provided in (Meleshenkovskii et al., 2018b). Application of CZT and $LaBr_3$(Ce) detectors for uranium enrichment determination tasks using the enrichment-meter method is discussed in (Vo, 2006; Berndt and Mortreau, 2017). However, there has yet been no comprehensive study that would assess the performance limits and possibilities of the enrichment-meter method with CZT and $LaBr_3$(Ce) in view of such factors as statistical quality of acquired spectra, region-of-interest (ROI) size as well as various methods used for the net peak area determination impact on the accuracy and uncertainty.

In this paper we aim to fulfill the mentioned scientific gap and broaden the existing research in the domain of room temperature medium resolution detectors, such as CZT and $LaBr_3$(Ce), for various tasks in safeguards applications. The goal of this paper is to investigate how different net peak area determination methods, peak shape models, symmetrical/asymmetrical ROI boundaries and statistical quality of the acquired spectra impact the method performance. We propose a methodology how the ROI boundaries can be setup, perform a sensitivity analysis and make recommendations on the best combinations of the ROI size and method used for the net peak area estimation for each of the tested detectors. Tests are conducted using spectra of CBNM (Central Bureau for Nuclear Measurements) certified uranium standards with the enrichment degrees from 0.31% to 4.46% of ^{235}U atomic abundance (Carpenter et al., 1986) on a 500 mm^3 CZT detector of a quasi-hemispherical design and a 2×2 inch $LaBr_3$(Ce) scintillator (Meleshenkovskii et al., 2017a), acquired for 7200 and 14400 s. The net peak area determination methods tested in this paper include a traditional three-window channel summation method as well as different analytical functions with a step-like background model. For asymmetrical peaks of the tested CZT detector we evaluate two different analytical peak shape model options – a tailed one and a single Gaussian based one.

The manuscript is organized as follows: Section 1 is devoted to introduction to the topic, Section 2 provides detailed information on the enrichment-meter method formalism, detectors, measurement setup, uranium standards and the proposed algorithm; Section 3 displays the results and Section 4 concludes the paper.

2. Methods and instruments

Application of passive gamma-ray spectroscopy in safeguards tasks involves analysis of the distribution of counts over the energy spectrum with a focus on X- and gamma-ray signatures of radioisotopes. A unique advantage of gamma-ray spectroscopy in safeguards tasks is its capability to extract the information from X- and gamma-ray signatures making a connection between the physical processes in the assaying material (such as decay, self-absorption and attenuation) and the corresponding isotopic composition. Over the years there has been developed a range of different methods that exploit the advantages of passive non-destructive X- and gamma-rays spectroscopy for the purposes of uranium and plutonium isotopic composition determination tasks in safeguards applications. Although, the conceptual principles of these methods can be different from each other, what underpins them from a methodological point of view is a rigorous coupling between the model used to describe the physical processes/interactions and a statistical tool used to analyze and interpret the corresponding experimental data. Such physical models are in general more constrained with respect to their parameters and functional behaviour, which is determined by the nature of the physical process/interaction they are applied to. As such, in passive X- and gamma-ray spectroscopy the fundamental physical premise is the proportionality of the observed net count rates in the full absorption photopeaks to the decay rates of the corresponding radioisotopes. By measuring of the net peak areas, taking into account the corresponding gamma-ray emission probabilities, counting efficiency and acquisition time one approaches the possibility to make a connection between the experimental data and corresponding isotopic composition of the radionuclides in the assaying material.

The mentioned physical premise is fundamental for the two widely used in safeguards methods for the determination of the uranium enrichment. Conceptually one of these methods is based on the isotopic ratios concept with an intrinsically calibrated counting efficiency curve,

the other one is known as the enrichment-meter method and requires calibration standards. However, since both of these methods use the same physical premise given by the proportionality of the observed net count rates to the decay rates, the key role is played by the statistical quality of the observed X- and gamma-ray signatures and the model used to measure the net peak areas. The latter requires selection of the corresponding ROI over which the net counts in a signature photopeak are determined. In that respect asymmetrical photopeaks of CZT detectors represent a challenge due to the presence of low-energy tailing.

2.1. Measurement instrumentation and uranium standards

Uranium spectra were measured on a 2×2 inch $LaBr_3(Ce)$ scintillator (FWHM @661 keV $\leq$2.9%, as specified by the manufacturer (Saint-Gobain Detectors leaflet 2019)), fabricated by Saint-Gobain Crystals and a 500 mm^3 CZT detector (FWHM @661 keV $\leq$2.5%, as specified by the manufacturer (Ritec Detectors Leaflet, 2019)), fabricated by Ritec.

A $LaBr_3(Ce)$ detector was coupled to a traditional analogue pulse processing chain instrumentation, consisting of a Canberra amplifier model 2024, Ortec high voltage power supply model 556 and Silena analogue-to-digital converter model 7423 UHS. Pulse processing chain parameters were set to 0.5 keV/channel gain, 0.5 μs shaping time. The high-voltage bias supplied to the detector was 590 V $LaBr_3(Ce)$ spectra were collected using DAQ2000 data acquisition software installed on PC.

A CZT detector was coupled to a digital pulse processing chain GBS Elektronik Multi Channel Analyzer (MCA), model 527. The high-voltage bias applied to the detector was 1400 V. The pre-amplifier signals were processed by MCA using trapezoidal shaping with 1.2 μs constant. The coarse gain setting was 10 and fine gain setting was 1.5, the trigger filter was (+1, 0, −2, 0, +1) and the flat top parameter was 1 μs. CZT spectra were collected using the WinSpec data acquisition software. Instrumentation was operated at room temperature in a laboratory environment with constant ambient background.

We used CBNM certified uranium standards with enrichment degrees ranging from 0.31% to 4.46% of ^{235}U atomic abundance. These standards were measured using lead collimators to satisfy the infinite thickness criteria required for the enrichment-meter method. The collimators were machined to meet the exact dimensions of the used CZT and $LaBr_3(Ce)$ detectors, as shown in Figs. 1 and 2.

The sample-to-detector distance parameter was kept constant for all measured uranium standards. A detailed information on the standards composition, geometry and packaging is provided in (Carpenter et al., 1986). Uranium spectra were acquired for 7200 and 14400 s on both detectors with 8192 channels spectrum size, as shown in Figs. 3 and 4 for a 7200 s case, to investigate the impact of the counting statistics on the method performance.

As can be seen from Figs. 3 and 4, the spectroscopic performance of the tested detectors is significantly different. A larger volume $LaBr_3(Ce)$ has superior counting statistics quality for the same acquisition time due to a significantly better counting efficiency. Due to the small size and hence poor counting efficiency, 500 mm^3 CZT detector measured uranium spectra are noticeably worse in their statistical quality, although

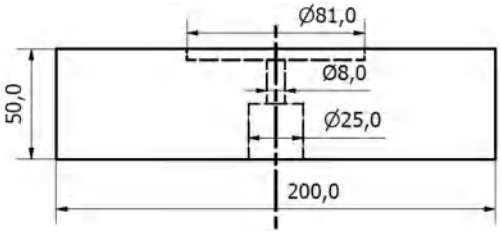

Fig. 1. CZT detector lead collimator.

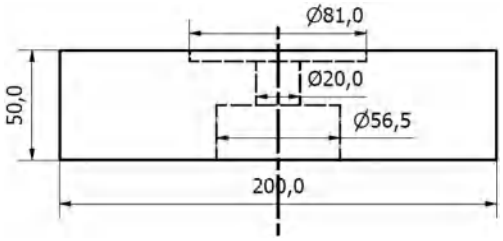

Fig. 2. $LaBr_3(Ce)$ detector lead collimator.

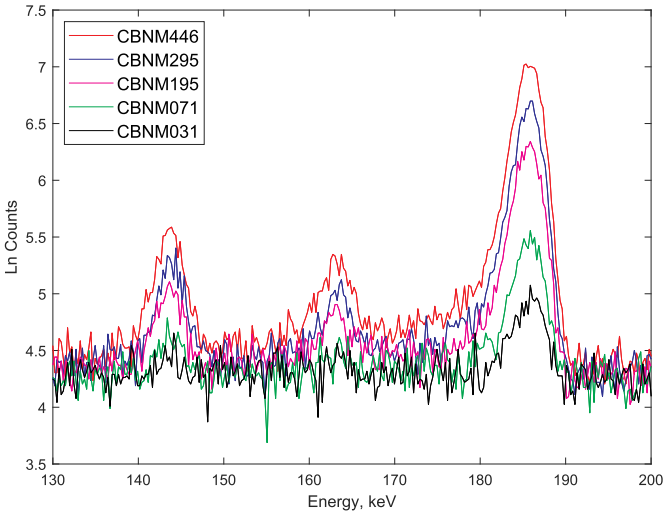

Fig. 3. CZT 143–185.7 keV ROI (7200 s).

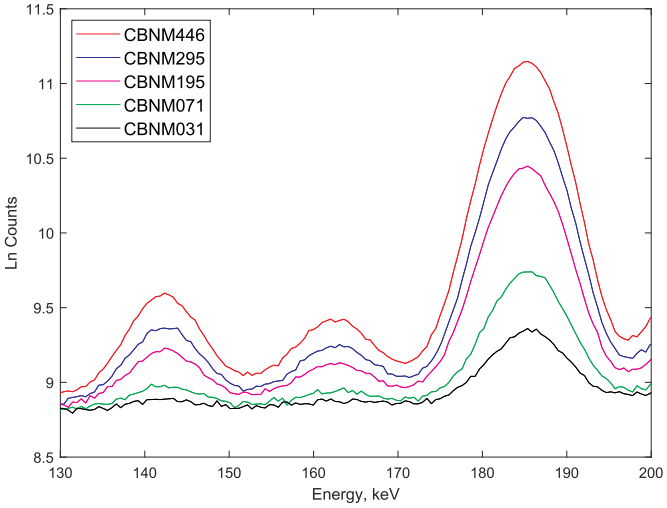

Fig. 4. $LaBr_3(Ce)$ 143–185.7 keV ROI (7200 s).

its energy resolution is better than that of a $LaBr_3(Ce)$. However, what is inherent for the spectroscopic performance of both tested detectors is that the most prominent 185.7 keV signature photopeak of ^{235}U is overlapped with its neighboring 182.6 keV.

A detailed description and analysis of the uranium standards measurement campaign is provided in our previous work (Meleshenkovskii et al., 2017a).

2.2. The enrichment-meter method

Determination of the uranium enrichment in absolute terms requires

complicated destructive methods based on mass-spectrometry or chemical analysis. In-field safeguards applications the preference is usually given to passive non-destructive methods. Among such different methods the most accurate results can be achieved with the so-called enrichment-meter method, in which the uranium enrichment is determined relative to a calibration standard (Matussek, 1985). Originally proposed in 1960s, this method was quickly employed for uranium enrichment determination tasks in a variety of applications thanks to its simplicity, robustness and compatibility with low-resolution instrumentation (Russell, 1968; Reilly et al., 1970; Parker and Reilly, 1972; Walton et al., 1974; Kull and Ginaven, 1974; Matussek, 1985; Smith, 1991).

The measurement procedure requires viewing of a uranium sample through a collimated channel with a gamma-ray detector. The method formalism is based on a premise that the net count rate in the 185.7 keV photopeak of ^{235}U is directly proportional to the enrichment (Matussek, 1985), as shown by equation (1).

$$Enr = k*NCR_{185.7}*C_m*C_w*C_l*C_{int} \quad (1)$$

where k is the calibration constant, $NCR_{185.7}$ is the net count rate in the 185.7 keV photopeak of ^{235}U radioisotope and C_m, C_w, C_l, C_{int} terms represent correction factors for the matrix attenuation, container wall attenuation, counting rate losses and gamma interference respectively. To account for the detection efficiency and geometrical factors a proportionality constant is determined from a measurement with a standard, the enrichment of which is known.

The net count rate in the 185.7 keV photopeak represents the portion of counts that lie over the background continuum below the photopeak. There are different methods for how the net count rate can be determined, they are classified on the two major methods: a singlet summation window method and a doublet summation method. The singlet summation window method excludes the 182.6 keV photopeak when summing the counts for the ROI window representing the 185.7 keV photopeak, whereas the doublet summation method includes it. The singlet method is usually used with high-resolution instrumentation, such as HPGe detectors, whereas the doublet method can be applied with any of the detectors. We would like to point out that for both methods different approaches for the net peak area determination can be used. These approaches can be based on an analytical function fit and a channel summation methods. The channel summation method is the simplest of the two. The analytical function fit implies fitting parameters in a model representing the peak shape. These fitting parameters result in associated uncertainties, which are reflected in the combined uncertainty on the net peak area.

If the uranium sample is large enough, the 185.7 keV gamma-rays from only a fraction of the total sample will reach the detector due to the strong sample self-absorption of typical uranium-bearing materials for this gamma-ray energy. This fraction is called *visible volume* of the sample, which is determined by the detector geometry and the mean free path of the 185.7 keV photons in the sample material and is defined by the collimator geometry. Such physical condition is known as the *infinite thickness* criterion. The mean free path and infinite thickness parameters for the 185.7 keV gamma-rays in most commonly assayed uranium materials are summarized in Table 1.

Where mean free path is proportional to $1/\mu\rho$ for a given material (μ is the attenuation coefficient and ρ represents the density of material) for the 185.7 keV gamma-rays, infinite thickness is defined as seven mean free paths for the 185.7 keV gamma-rays in the material. Since the infinite thickness criterion limits the visible volume of the sample, the enrichment-meter method can only assay the surface of a uranium sample. For such enrichment measurements to be meaningful for the given visible volume, the material of a uranium sample must be isotropically uniform. If the latter condition cannot be satisfied, non-homogeneity corrections must be introduced. However, in many practical applications of the enrichment-meter method the infinite-thickness criterion is satisfied with quite reasonable sample sizes.

Table 1
Mean free paths and infinite thickness parameters for common uranium materials[a].

Uranium material	Density, g/cm^3	Mean free path, cm	Infinite thickness, cm
Metal	18.7	0.04	0.26
UF_6 (solid)	4.7	0.2	1.43
UO_2 (sintered)	10.9	0.07	0.49
UO_2 (powder)	2	0.39	2.75
U_3O_8 (powder)	7.3	0.11	0.74
Uranyl nitrate	2.8	0.43	3.04

[a] (Reilly et al., 1991).

Thus, if samples with unknown enrichment have the same physical distribution, matrix material, packaging and measurement geometry the enrichment can simply be determined by multiplication of the measured net count rate in the 185.7 keV photopeak in their spectra by the proportionality constant, which can be achieved by simplifying equation (1) to a form as given by equation (2):

$$Enrichment = k*NCR_{185.7} \quad (2)$$

In cases when the physical parameters of the measured samples differ, it is necessary to introduce corrections (Berndt and Mortreau, 2017). Although being specifically suited for NaI detector performance, the NaIGem code allows for built-in procedures necessary for such corrections (Gunnink, 2001).

One of the considerable advantages of the enrichment-meter method for the determination of the uranium enrichment is that it utilizes the information from a single ROI. Besides, this method is considered one of the most accurate passive non-destructive methods for the determination of the uranium enrichment. However, its application is limited to those cases when the calibration standards can be provided and it can be only used with uranium materials.

2.3. The ROI boundaries selection algorithm

Asymmetrical photopeaks of CZT detectors require not only a suitable method for net peak area determination but also carefully selected ROI boundaries to perform either a function fit or a channel contents summation routine. However, the size of the ROI window depends on the energy resolution of the detector and requires a particular attention in cases when the peak shape is asymmetrical. The latter can have an impact on the method performance making it sensitive to the choice of the ROI boundaries.

Since the underlying mathematical formalism of energy deposition in X- and gamma-ray detectors implies Gaussian nature of the broadening events, analytical peak shape models always have a central Gaussian part centered around the peak maximum energy (Gilmore, 2008). Consequently, a robust ROI window selection algorithm can be based on the actual parameters of such distributions, individual to any given detector. Thus, to fully describe a Gaussian distribution, one needs to specify the expected mean and standard deviation. In spectroscopic terms these parameters represent the channel number corresponding to the peak maximum energy and FWHM, which is related to the standard deviation as $FWHM = 2.355\sigma$, where σ is the Gaussian standard deviation. The corresponding one standard deviation boundaries represent 68.3% of the peak area.

However, for the net peak area determination ROI intervals may represent a particular challenge due to the low-energy tailing part of the photopeak and determination of the background levels at the photopeak boundaries. These aspects become in particular important for detectors of low- and medium energy resolution and asymmetrical photopeaks of CZT detectors. We developed the following ROI selection algorithm, as schematically shown in Fig. 5.

The algorithm starts with an energy calibration routine necessary for

the photopeak identification. After the signature photopeaks were identified using the channel of the photopeak maximum count, the coarse ROI boundaries are selected arbitrarily. Coarse selection implies that photopeak region is fully covered, however without any specific information on the exact ROI boundaries to satisfy the strict statistical formalism (e.g. 1σ, 2σ etc.). Then a Gaussian function is fitted to the selected coarse ROI boundaries repeatedly in a routine of n-iterations. This fitting aims at determining the peak parameters and fluctuation of their absolute values as a function of coarse ROI interval range. Since the mathematical formalism of a Gaussian function implies that it can be fully described by its mean and standard deviation parameters, such fitting allows for a robust determination of the respective parameters. For a preselected number of coarse runs the mean values of parameters are calculated using the 95% confidence interval. Those values that fall within this interval are taken to average the parameter values to return the mean value of the centroid position and standard deviation for a given photopeak.

Using the determined parameter values ROI boundaries for $n\sigma$ intervals are calculated using the formalism of *expected mean* $\pm\, n\sigma$. To recommend a particular ROI interval for each of the tested detectors we have conducted sensitivity analysis of the ROI interval selection and its impact on the fitting statistics and the net peak area uncertainty.

2.4. The net peak area determination methods

There are different methods how the net peak area can be determined (Matussek, 1985; Carpenter et al., 1986; Reilly et al., 1991; Gilmore, 2008). They can be divided into three large groups – those that require peak fitting using a suitable closed-form analytical peak shape model, those that are based on the so-called physics-based peak shape models and those that are based on a counting window channel summation method. The first requires elaborate peak shape and background models, the second is most complex in its calculation routines and is based on estimation of all sequential processes that contribute to energy deposition. The third one is the simplest and can be realized in two- or three-window arrangement. However, fitting of an analytical peak shape model implies a number of fitting parameters in it as well as in the function used to describe the background continuum. These free parameters inevitably become additional sources of the net peak area uncertainty.

2.4.1. Analytical function fit

An important requirement for a peak shape model used for the net peak area determination is its adequate approximation of the peak shape behavior as a function of energy (Helmer and Lee, 1980). Traditionally, to approximate gamma-ray peaks, Gaussian-based peak shape models are widely used with both semiconductor and scintillation detectors (Routti and Prussin, 1969; Mcnelles and Campbell, 1975; Helmer and Lee, 1980). The premise for using a Gaussian-based peak shape model arises from the physical particularities of charge induction and collection processes in the sensitive volume of the detector, the statistical behavior of which in its essence tends to be Gaussian in nature (Routti and Prussin, 1969). To approximate the portion of charges that contribute to the full absorption gamma-ray peak a Gaussian function is used (Routti and Prussin, 1969; Helmer and Lee, 1980). However, to account for the charges that do not contribute to the full absorption peak due to losses in charge collection mechanisms and trapping, a low-energy tailing model is added to the central Gaussian part (Routti and Prussin, 1969; Mcnelles and Campbell, 1975; Helmer and Lee, 1980). The functional form of such a tailing model can be represented by different classes of functionals, which can be based on exponential or error corrected closed-form functions (Routti and Prussin, 1969; Helmer and Lee, 1980). For HPGe detectors the portion of charges that leads to tailing is not significant (Routti and Prussin, 1969; Helmer and Lee, 1980), whereas for a room temperature CZT detector they can exhibit a significant portion (Nambooridi et al., 1996; Arlt and Gunnink, 2001). However, same mathematical formalism to account for the tailing contribution can be used for CZT detectors.

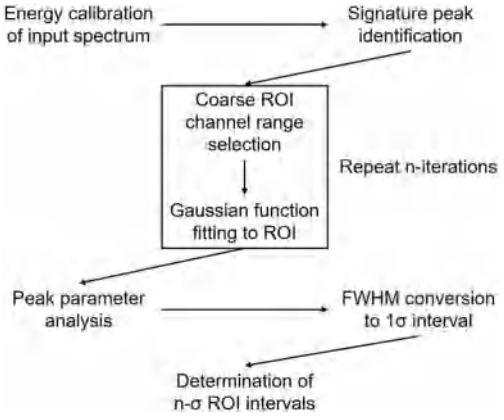

Fig. 5. ROI selection algorithm flow chart diagram.

2.4.1.1. Gaussian peak shape model. A parametrized Gaussian peak shape model is given by equation (3):

$$y_i = \left(\frac{A}{w^*\sqrt{\pi/2}}\right) * exp\left(-2*\frac{(x_i - x_0)^2}{w^2}\right) \tag{3}$$

$$w = FWHM \Big/ \sqrt{ln(4)}$$

where y_i represents the content at channel i, A is the peak area parameter, w is the peak width parameter, x_i is the channel number, x_0 is the centroid position of the peak and *FWHM* is the full width at half maximum.

To describe the Compton background under the peaks we used a step-like function (4) (Helmer and Lee, 1980).

$$BKG(i) = \left[\left(\frac{1}{2} * erfc\left[\frac{(x_i - x_0)}{\sqrt{2}*w}\right]\right) * a\right] + b \tag{4}$$

where BKG_i is the background content at channel i, x_i is channel i, x_0 is the centroid position of the peak, w is the peak width parameter, a is the background step height parameter and b is the background offset parameter.

The peak fitting routine implies fitting of equations (3) and (4) to the 185.7 keV photopeak in measured uranium spectra using a gradient-based Levenberg-Marquardt (Marquardt, 1963; Moré, 1977) technique according to a minimization criterion, given by equation (5)

$$\chi^2_R = \frac{1}{n}\sum_{roi\_l}^{roi\_r}\left[\frac{exp_i - model_i}{\sigma_i}\right]^2 \tag{5}$$

$$n = roi_r - roi_l + 1 - NPAR$$

where *roi_l*, *roi_r* specify the fitting interval (region of interest); *NPAR* is the number of degrees of freedom (number of fitting parameters); $model_i$ is the analytic approximation at channel i, exp_i is the counts at channel i and σ_i is the variance.

To derive the uncertainties on the peak shape model parameters we have used the Jacobian matrix returned by the built-in *lsqnonlin* optimization solver of Matlab to estimate the asymptotic covariance matrix (Brown, 2001; Hu et al., 2015) (V), as shown by equation (6):

$$V = \sigma^2 * (J^* J)^{-1} \tag{6}$$

where J is the Jacobian matrix returned by the *lsqnonlin* optimization solver. The σ^2 was approximated by dividing *SSE* by the number of

degrees of freedom, *df*, as shown by equation (7) (Hu et al., 2015):

$$\sigma^2 = \frac{SSE}{df} \tag{7}$$

where *SSE* is the sum squared error calculated from the fitted peak shape model residuals and *df* is calculated as the number of channels in the ROI of the fitted peak minus the number of peak shape model fitting parameters.

2.4.1.2. Exponential tail peak shape model. Peak asymmetry of a 500 mm^3 CZT detector for energies beyond 200 keV becomes significant, removing the possibility to use a single Gaussian peak shape model. Such asymmetry has a non-linear behavior as a function of energy and requires a corresponding low-energy tailed peak shape model. However, although for the tested CZT detector the peak shape at 185.7 keV energy has a slight asymmetry, for larger volume CZT detectors it can be more pronounced. In this paper, we thus present the formalism to address such cases. To account for low-energy asymmetry various low-energy tailed peak shape models can be used. Such models are Gaussian-based, however the tailing component can be described by different functionals (Routti and Prussin, 1969; Helmer and Lee, 1980; Arlt and Gunnink, 2001). One of the ways to account for such low-energy tailing is to use a truncated tailing model described by an exponential function. The choice of an exponential functional form for the tailing component is suggested by the empirical behavior of the gamma-ray interaction processes in compound semiconductor detectors, such as CZT. Indeed, it was shown by (Sato et al., 2002) that incident gamma-ray photons are attenuated with an exponential-form decay as a function of gamma-ray energy, as given by equation (8):

$$N = N_0 exp\left(-\frac{x}{\lambda(E_\gamma)}\right) \tag{8}$$

By differentiating of equation (8), the ratio of photons which interact at the region between x and $x + dx$ can be determined, as shown by equation (9):

$$-\frac{dN}{dN_0} = \frac{1}{\lambda(E_\gamma)} exp\left(-\frac{x}{\lambda(E_\gamma)}\right) dx \tag{9}$$

where N_0 is the number of photons of given energy that reach the detector surface, N represents the number of photons of given energy that reach region x, x is the depth from the detector surface and λ is the mean free path by photo absorption as a function of energy of the incident gamma-ray.

In this paper we investigate the performance of such a tailed peak shape model with seven fitting parameters and a single tailing component expressed by an exponential, as shown by equation (10):

$$y_i = y_o * \left[e^{-\alpha*(x_i - x_0)^2} + T(x_i)\right] \tag{10}$$

$$\alpha = \frac{4*ln(2)}{FWHM^2}$$

$$T(x_i) = \left[A * e^{B*(x_i - x_0)}\right] * \left[1 - e^{t*\alpha*(x_i - x_0)^2}\right] * \delta$$

$$\delta = 1 \ if \ x_i < x_0$$

$$\delta = 0 \ if \ x_i \geq x_0$$

where y_i represents the content at channel i, y_0 is the peak amplitude parameter, α is the peak width parameter, *FWHM* is the full width at half maximum, x_i is the channel number, x_0 is the centroid position of the peak, $T(x_i)$ is the tailing component at channel i, A is the tailing amplitude parameter, B is the tailing slope parameter and delta term δ limits the tailing contribution only at the low energy side of the peak. The truncation parameter t controls the bounding of the tailing component and was set to *0.6* as recommended in the literature for asymmetrical peaks (Arlt and Gunnink, 2001).

The behavior of such a truncated peak shape model is shown in Fig. 6. Due to truncation at the peak maximum energy the contribution of the tailing component to the photopeak is limited to the low-energy side of the photopeak exclusively. The relative area of the tailing component is thus significantly smaller than the Gaussian area.

The peak fitting routine was realized using a gradient-based search Levenberg-Marquardt (Marquardt, 1963; Moré, 1977) technique in the same way using the same model to describe the Compton continuum under the photopeaks, as described in section 2.4.1.1.

To derive the uncertainties on the peak shape model parameters we have used the Jacobian matrix returned by the built-in *lsqnonlin* optimization solver of Matlab as described in section 2.4.1.1. However, unlike the single Gaussian model, a single-tailed peak shape model does not have a peak area parameter embedded in it. To propagate the uncertainty on the resulting net peak areas when using a single-tailed peak shape model we used a Monte Carlo realization of the Taylor expansion technique (Fox and Weisberg, 2010). In such a technique, the fitting parameters are sampled within their one sigma uncertainty interval, computed from the covariance matrix as described above. For each sample of the fitting parameters ensemble, the corresponding net peak area is computed by integrating the peak shape model. Such routine is repeated in a series of *n*-iterations. The resulting posterior distribution of the net peak area values allows to estimate the standard deviation.

2.4.2. Three window channel summation

Another well-known method for the net peak area determination is the so-called channel summation method. In its essence, it represents selection of three windows – one around the peak and two at its boundaries. The two background windows at the peak boundaries are used to linearly interpolate the background under the selected ROI. The size of such windows depends on the energy resolution of the detector and interference with neighboring photopeaks. Usually no less than three are used (Gilmore, 2008) to average the background offset at the right boundary and step-height at the left boundary. Then, a summation of channel contents over the entire ROI is performed to estimate the gross count, followed by subtraction of the background portion determined from the linear interpolation.

Energy resolution of a 500 mm^3 room temperature CZT detector yields a relatively detailed information on the major ^{235}U gamma-ray signatures in the 143–186 keV energy range and thus allows using of the channel summation method for net peak area determination. In this

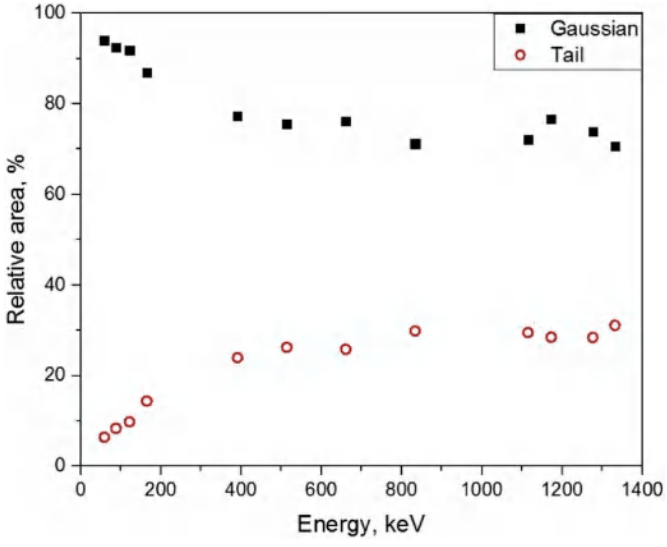

Fig. 6. 500 mm^3 CZT detector truncated exponential tail behavior.

work we used the following mathematical formalism, as given by equation (11):

$$A = \sum_{i=ROI_L}^{ROI_R} C_i - n\left[\sum_{i=ROI_L-m}^{ROI_L-1} C_i + \sum_{i=ROI_R+1}^{ROI_R+m} C_i\right] \Big/ 2m \quad (11)$$

where A is the net peak area of the ROI, ROI_L and ROI_R are the corresponding boundaries, C_i is the gross content at channel i, n is the number of channels within the ROI region, m is the number of channels used to average the background offset and step-height at the ROI boundaries.

The uncertainty on the derived net peak area was propagated as given by equation (12):

$$\sigma_A = \sqrt{\sum_{i=ROI_L}^{ROI_R} C_i + n^2\left[\sum_{i=ROI_L-m}^{ROI_L-1} C_i + \sum_{i=ROI_R+1}^{ROI_R+m} C_i\right] \Big/ 4m^2} \quad (12)$$

A particular advantage of a three-window channel summation method, besides its simplicity, is that there are no additional influences on the net peak area uncertainty due to the fitting parameters uncertainty and covariance, as well as no impact of their functional behavior with respect to the counting statistics quality. However, it should be mentioned that such a method does not allow for deconvolution of photopeaks subject to significant overlapping.

In this work, in section 3.2 we present the sensitivity study of the enrichment-meter method performance to the different sizes of the central ROI window as well as different sizes of the background windows used for background levels averaging.

2.5. Combined uncertainty propagation

To propagate the combined uncertainty on the determined enrichment the following expression was used (13):

$$\sigma_{Enr} = \sqrt{Enr^2 * \left[\left(\frac{\sigma_{NCR_{185.7}}}{NCR_{185.7}}\right)^2 + \left(\frac{\sigma_k}{k}\right)^2\right]} \quad (13)$$

where σ_{Enr} is the uncertainty on the determined enrichment, σ_{NCR} is the net count rate uncertainty for the 185.7 keV gamma peak of ^{235}U radioisotope, NCR is the net count rate in the 185.7 keV gamma peak of ^{235}U radioisotope, σ_k is the uncertainty on the proportionality constant, k is the value of the determined proportionality constant.

The uncertainty on the declared enrichment values was less than 0.1% (Carpenter et al., 1986) and was not included in the calculations.

3. Results and discussion

3.1. Calibration constant

As it was discussed in section 2, the enrichment of unknown samples is determined by multiplying the measured net count rates in the 185.7 keV ROI by the proportionality constant. There are different methods how this proportionality constant can be determined. Thus, usually a linear fit is performed on the experimental net count rate data points obtained from calibration standards (Matussek, 1985), as shown by equation (14):

$$Enr = (a * NCR_{185.7}) + b \quad (14)$$

where a and b are the slope and offset coefficients, $NCR_{185.7}$ is the net counting rate in 185.7 keV photopeak. However, such linear fit requires a set of calibration standards to allow for at least one degree of freedom. In the work presented in this paper we were limited to only five uranium standards. To test the performance of the enrichment-meter method we thus used one standard as a calibration one, whereas other standards were assumed to have unknown enrichment values. In such a case, the proportionality constant k can be determined algebraically by rearranging equation (2) from a calibration measurement with a standard the enrichment of which is known, as shown by equation (15). The uncertainty on the proportionality constant is influenced by the uncertainty on the experimental net count rate of the calibration standard and was determined by differentiation of equation (15), as shown by equation (16).

$$k = \frac{Enrichment}{NCR_{185.7}} \quad (15)$$

$$\sigma_k = \sqrt{k^2 * \left(\frac{\sigma_{NCR_{185.7}}}{NCR_{185.7}}\right)^2} \quad (16)$$

In this work, we used the CBNM446 with 4.46% of the corresponding ^{235}U atomic abundance respectively as the calibration standard.

3.2. Sensitivity assessment

The enrichment-meter method requires determination of the net count rate in a ROI corresponding to the 185.7 keV gamma-ray signature of ^{235}U. Different approaches could be used – either a doublet summation or a singlet, the choice between which depends on the energy resolution of the detector. However, different methods are possible for actual net peak area determination. Since the enrichment depends on the net peak area, the method used for the net peak area determination will affect the corresponding accuracy and uncertainty.

Because the energy resolution of both tested detectors is worse than that of HPGe, we have used a doublet summation approach with two different methods for the net peak area determination – an analytical function fit and a three-window channel summation method. For the $LaBr_3$(Ce) detector due to its symmetrical photopeaks we have used a Gaussian analytical function, whereas for the CZT detector two different analytical functions were tested – a Gaussian and a tailed Gaussian described in section 2.4.1.2.

3.2.1. $LaBr_3$(Ce) detector

Net count rates determined using an analytical function fit and a three window channel summation method for a 2 × 2 inch $LaBr_3$(Ce) detector for different sizes of ROI are presented in Table 3. The selected ROI represents a doublet which includes both a 182.6 keV and a 185.7 keV photopeaks, which given the energy resolution of a $LaBr_3$(Ce) detector are overlapped. For the three window channel summation method fifteen channels were used at the background windows to average the background levels. As can be seen from Table 2, for a 4σ ROI window resulting net peak area uncertainties are lower by approximately a factor of two. Such behavior is due to the fact that in an analytical model parameters corresponding to the background step and offset converge better when the tails of the Gaussian distribution have asymptotically reached the background continuum. In case of a 3σ ROI the tails of the Gaussian distribution still contain some information corresponding to the photopeak and thus influence the variance in the channels corresponding to the background. The effect is especially pronounced for low-enrichment uranium standards, in which due to the low content of ^{235}U radioisotope its signatures are very close to the background continuum. However, for a channel summation method the situation is different. Thus, increase of the central ROI window to 4σ sigma negatively affects the uncertainties. Such behavior is because for a channel summation method besides the central ROI window the two background windows must contain at least from three to five channels to interpolate its levels. The latter inevitably overlap with channel contents in the closely neighboring photopeaks given the energy resolution of a $LaBr_3$(Ce) detector. We believe that for other sizes of $LaBr_3$(Ce) scintillator family, due to different signal-to-noise ratio and therefore background continuum this performance may be different, which can be an interesting premise for future research.

Where NCR is the net count rate in the ROI corresponding to the

Table 2
$LaBr_3$(Ce) detector CBNM net count rates (7200 s).

CBNM standard	7200 s acquisition time							
	Function fit				Three-window channel summation			
	3σ ROI		4σ ROI		3σ ROI		4σ ROI	
	NCR, counts/s	Std, rel. %	NCR, counts/s	Std, rel. %	NCR, counts/s	Std, rel. %	NCR, counts/s	Std, rel. %
446	167.87	0.86	166.56	0.56	155.29	0.13	152.76	0.14
295	112.08	1.03	110.57	0.62	102.86	0.17	101.28	0.19
194	72.53	1.20	72.80	0.70	68.55	0.23	67.43	0.26
071	26.87	2.28	26.64	1.03	25.81	0.48	25.61	0.56
031	12.19	4.07	12.01	1.82	11.91	0.93	11.86	1.14

Table 3
$LaBr_3$(Ce) detector CBNM446 sensitivity study.

3σ ROI background window variation, channels	7200 s acquisition time	
	Gaussian function fit	
	NCR, counts/s	Std, rel. %
+1	167.64	0.76
+2	167.21	0.69
+3	167.32	0.63
+5	166.85	0.57

182.6 keV–185.7 keV doublet.

A two-fold increase in the acquisition time reduces the net peak area uncertainties for both net peak area determination methods. However, its effect is negligible compared to the effect given by selection of a *4σ* ROI instead of a *3σ* ROI one.

Results of a sensitivity study for an analytical model fitted to the different ROI boundaries are presented in Table 3 for the CBNM446 standard, as an example. As can be seen from the table, due to symmetrical photopeaks in $LaBr_3$(Ce) spectra, the variation in the determined net count rates in a specified ROI is within the uncertainty range of the fixed *3σ* and *4σ* ROI boundaries. Such behavior was observed for all uranium standards tested.

Sensitivity assessment for a channel summation method is based on the number of channels taken for background levels averaging at the two background windows. In the literature (Gilmore, 2008) no less than three channels are recommended. Thus, to address the sensitivity of the channel summation method applied to a 2 × 2 inch $LaBr_3$(Ce) detector we have set the following range of channels at the two background windows: three, five, ten and fifteen. The results presented in Table 4 for the CBNM446 standard indicate that there is no improvement in the uncertainties on the determined net count rates for the number of channels beyond ten, which is in good agreement with the results of (Gilmore, 2008). However, the situation changes when a *4σ* interval is chosen for the center ROI window. In such a case the determined net peak area value becomes very sensitive to the choice of the number of channels in the background windows used to average the background levels, as shown in Table 5 for the CBNM446 standard. Such behavior is because a wider *4σ* central ROI window represents 99.9% of the total Gaussian representing the 185.7 keV photopeak (overlapped with a 182.6 keV photopeak) which is very close to the 143 keV and 202–205 keV photopeaks. Thus, a large number of channels taken to average the background levels at the peak boundaries inevitably includes channel contents of the neighboring photopeaks.

3.2.2. CZT detector

In section 1 asymmetrical photopeaks of a 500 mm^3 CZT were discussed. Although such an asymmetrical shape has a nonlinear behaviour as a function of energy as it was shown in section 2, for energies below 200 keV it is possible to use a Gaussian peak shape model since the asymmetry at these energies is not yet severe. We would like to clarify that such behavior was observed for the tested 500 mm^3 CZT detector of a quasi-hemispherical design and can be different for other types/sizes of CZT detectors. Thus, at this energy the following analytical function options are possible: a Gaussian as well as a more elaborate tailed peak shape models. Besides, a traditional three-window channel summation method can be used as well. The former two were coupled with a step-like function to describe the Compton background under the peak, for the latter a linear interpolation was used.

Performance assessment of the enrichment-meter method with a CZT detector was conducted using the mentioned options for the net peak area determination. Besides, we have assessed the sensitivity of each of the methods to the ROI interval size, including its asymmetrical options. For the three-window channel summation method we have additionally investigated how the number of channels at the peak boundaries used to average the background levels impacts the net peak area value and its uncertainty. The asymmetrical photopeaks of a CZT detector set a particular requirement for the ROI interval selection when using a three-window channel summation method. This is because the model used to interpolate the background is linear and a slight asymmetry at the left boundary may influence the corresponding background level and impact the determined net peak area, which in terms of the linearity between the net count rate and sample enrichment has a direct impact on the method performance.

For a single Gaussian function fit we evaluated two different options for the ROI interval – a *3σ* one and a *4σ* one. The former covers 99.7% of the counts in the photopeak area, the latter covers 99.9% of the counts. For both ROI intervals the exact channels representing the selected boundaries were determined using the proposed ROI selection algorithm, as described in section 2.3. The quantitative parameters used to evaluate the performance were the net peak area values and their corresponding uncertainties, as summarized in Table 6 for the tested

Table 4
$LaBr_3$(Ce) detector CBNM446 sensitivity study 3σ ROI interval.

# channels at the peak background windows	7200 s acquisition time	
	Channel summation method	
	NCR, counts/s	Std, rel. %
3	148.86	0.19
5	152.07	0.16
10	155.64	0.13
15	155.29	0.13

Table 5
$LaBr_3$(Ce) detector CBNM446 sensitivity study 4σ ROI interval.

# channels at the peak background windows	7200 s acquisition time	
	Channel summation method	
	NCR, counts/s	Std, rel. %
3	161.59	0.20
5	160.63	0.17
10	156.95	0.15
15	152.76	0.14

uranium standards.

Results indicate, that for both ROI intervals the determined net peak area value is within its uncertainty range. A *4σ* ROI interval yields smaller uncertainties, approximately of a factor of two for all uranium standards tested. Such behavior is due to better convergence of the fitting routine because at such an interval it is easier to fit the left and right background levels.

Sensitivity assessment results for a Gaussian analytical model are presented in Table 7 for CBNM446 standard, as an example. The same mathematical formalism as with similar tests conducted for the $LaBr_3(Ce)$ was used.

Situation with a tailed peak shape model is more complicated. As it was explained in section 2.4.1.2, such a model implies a larger number of fitting parameters which inevitably impact the combined uncertainty on the determined net count rate value (Meleshenkovskii et al., 2017b). Besides, with our results we find that such a model is highly sensitive to the ROI interval that it is fitted to and that such interval has a dependency on the statistical quality of the photopeak. The latter factor is directly related to the sample enrichment because for natural and depleted uranium standards the 185.7 keV signature photopeak is very close to the background continuum. Closeness to the background continuum yields higher degree of parameter correlation in the fitting procedure, in particular interference of the central Gaussian parameters with the tailing parameters. The low-energy tailing part is difficult to distinguish over the background noise and, consequently yields larger uncertainties on the parameters. The results summarized in Table 8 indicate that for a 4.46% enriched standard the single tailed model can be fitted for a ROI interval starting from *5σ*. For less enriched standards the recommended ROI interval increases to *6σ*. However, as can be seen from Table 8, even for large ROI intervals of *7σ* and *8σ* the net peak area uncertainties are noticeably larger than those achieved for a Gaussian fit using either *3σ* or *4σ* sigma ROI intervals. Such a behavior is observed due to the mentioned influence of an increased number of fitting parameters and statistical quality influence on the tailing component.

Another option for a tailed peak shape model is to use an asymmetric ROI interval. Since the asymmetry affects only the low-energy part of the peak, the corresponding window can be extended respectively to the left of the photopeak, keeping the right boundary fixed. Results for such asymmetrical ROI intervals are summarized in Table 9 for the CBNM446 standard. These results indicate that although the left ROI boundary remains at the level of *5σ* and *6σ*, the right boundary indeed can be reduced to a *3σ*. The resulting net count rate uncertainties reveal that there is no performance improvement when using such asymmetrical ROI intervals at this gamma-ray energy over symmetrical ones. As can be deduced from Table 9, to keep the net peak area uncertainty at the level achieved for symmetrical ROI intervals of *7σ* and *8σ*, asymmetrical ROI boundary at the left outlier has to be in the range from *9σ* to *10σ*.

However, we would like to point out that these results were achieved for a 185.7 keV gamma-ray energy, at which the asymmetry is not yet significant for a 500 mm^3 CZT detector of a quasi-hemispheric design. At higher energies the situation may change in favor of an asymmetrical ROI interval. Besides, we believe that for larger volume CZT detectors asymmetrical ROI interval may be required at 185.7 keV. A dedicated case-study is necessary.

Although a three-window channel summation method is the simplest method for the net peak area determination it can be quite sensitive to the choice of window intervals, especially when it is applied to asymmetrical peak shapes, such as of CZT detectors. Because the photopeaks are slightly low-energy tailed at this energy, the counts on the left background window become influenced by such tailing, which may negatively impact the averaging of the background level. To investigate the sensitivity we have conducted the following assessment. First, given the slight asymmetry at 185.7 keV energy the size of the central ROI window was investigated for *3σ*, *4σ*, *5σ*, *6σ* and *7σ* ROI boundaries. For each of the sizes of the central ROI window we have analyzed a different number of channels at the two background windows – from three to a maximum of fifteen. Table 10 indicates that for a *3σ* to *5σ* central ROI size the net peak areas are noticeably influenced by the low-energy tailing, which affects the number of averaged counts on the left boundary and makes the net peak area value monotonically increase with increasing number of the averaging channels. Only when the size of the central window is selected large enough, thus including the low-energy tailing part in it, the number of channels used to average the background level at the ROI boundaries does not impact the net peak area values. Such behavior was observed only for the central ROI window size starting from *6σ*.

We would like to point out, that the observed behavior is unique to the spectroscopic performance of the tested CZT detector and can be a function of its size and design. We believe that for other CZT sizes/designs the performance of a channels summation method may be different with respect to the effective ROI boundaries size.

Table 6
CZT detector CBNM net count rates (7200 s).

CBNM standard	7200 s acquisition time			
	Gaussian function fit			
	3σ ROI		4σ ROI	
	NCR, counts/s	Std, rel. %	NCR, counts/s	Std, rel. %
446	2.23	4.85	2.24	2.44
295	1.42	6.38	1.44	3.35
194	1.03	8.18	1.04	3.82
071	0.39	13.36	0.37	5.77
031	0.16	20.71	0.18	10.32

Table 7
CZT detector CBNM446 sensitivity study.

3σ ROI background window variation, channels	7200 s acquisition time	
	Gaussian function fit	
	NCR, counts/s	Std, rel. %
+1	2.21	3.94
+2	2.22	3.33
+3	2.22	2.92
+5	2.23	2.29

Table 8
CZT detector CBNM446 sensitivity study.

ROI interval	7200 s acquisition time	
	Single-tailed Gaussian function fit	
	NCR, counts/s	Std, rel. %
5σ	2.46	9.03
6σ	2.46	7.25
7σ	2.49	6.89
8σ	2.49	6.06

Table 9
CZT detector CBNM446 sensitivity study.

Asymmetrical ROI interval, left-right	7200 s acquisition time	
	Single-tailed Gaussian function fit	
	NCR, counts/s	Std, rel. %
6σ-3σ	2.42	9.62
7σ-4σ	2.49	8.96
8σ-5σ	2.49	7.02
9σ-6σ	2.52	6.37
10σ-6σ	2.52	6.03

Table 10
CZT detector CBNM446 sensitivity study.

# channels at the peak background windows	7200 s acquisition time									
	Channel summation method									
	3σ ROI interval		4σ ROI interval		5σ ROI interval		6σ ROI interval		7σ ROI interval	
	NCR, c/s	Std, rel. %	NCR, c/s	Std, rel. %	NCR, c/s	Std, rel. %	NCR, c/s	Std, rel. %	NCR, c/s	Std, rel. %
3	2.04	1.44	2.30	1.38	2.38	1.52	2.43	1.65	2.42	1.85
5	2.09	1.23	2.31	1.20	2.41	1.27	2.44	1.38	2.47	1.48
10	2.17	1.03	2.35	1.03	2.41	1.09	2.45	1.15	2.49	1.21
15	2.21	0.97	2.37	0.97	2.44	1.01	2.46	1.06	2.49	1.10

3.3. Results of the enrichment determination

To investigate the performance of a 500 mm^3 CZT and a 2 × 2 inch $LaBr_3(Ce)$ detectors with the enrichment-meter method, the net count rates in the 185.7 keV ROI were determined by a single Gaussian fit and a three window channel summation method. Net count rates used for calibration constants and enrichment determination were calculated using a *3σ* ROI for the Gaussian function fit for both detectors, *3σ* with $LaBr_3(Ce)$ detector and *6σ* with CZT detector for the channel summation method.

Determined enrichment values for different net peak area determination methods are presented in Tables 11 and12 for a 2 × 2 inch $LaBr_3(Ce)$ and for a 500 mm^3 CZT detector respectively. The acquisition time was 7200 s for all results presented. The accuracy on the determined enrichment was calculated according to equation (17).

$$Bias(\%) = \left[\frac{E_{det} - E_{dec}}{E_{dec}}\right] * 100 \quad (17)$$

where E_{det} and E_{dec} represent the determined and declared enrichment respectively.

Results of our study indicate that in terms of accuracy for the 185.7 keV photopeak of a 500 mm^3 CZT detector a single Gaussian peak shape model is advantageous when compared to a tailed peak shape model. However, as we have already explained above, such behavior is exclusive to the tested CZT detector model and size. We assume that for larger CZT detectors the asymmetry may be more pronounced at this energy and a tailed peak shape model with asymmetrical ROI boundaries may become advantageous. However, the simplest channel summation method with a *6σ* ROI boundary and from ten to fifteen channels taken to average the background level yields not only better uncertainties, but also in terms of accuracy it performed best of all cases investigated. Thus, a channel summation method can be a method of choice for the net peak area determination when using a 500 mm^3 CZT detector with the enrichment-meter method.

As can be seen from the results for a 2 × 2 inch $LaBr_3(Ce)$ detector, compared to a smaller CZT detector it displayed superior performance using *3σ* ROI boundaries with both tested methods for the net peak area determination. Such behavior is due to its symmetrical peak shapes and significantly better counting efficiency yielding smaller net peak area uncertainties.

4. Conclusions

Asymmetrical photopeaks of the tested CZT detector require an elaborate routine for ROI boundaries selection. The results of our study indicate that below 200 keV a single Gaussian peak shape model adequately fits photopeaks of a 500 mm^3 CZT detector. Thus, below 200 keV ROI boundaries can be restricted to *3σ* and *4σ* interval. At higher energies to adequately fit the tailing part of the photopeaks a significant extension up to *10σ-12σ* is required. However, the right outliers of CZT photopeaks at high energies can be fixed at a level of *5σ*, allowing to use asymmetrical ROI boundaries. The proposed ROI selection algorithm accounts for such asymmetrical photopeaks. However, we would like to point out that such performance was achieved for a 500 mm^3 CZT detector. We believe that for larger volume CZT detectors of same design and/or other designs of CZT detectors performance of the tested peak shape models can be different. A dedicated case-study is necessary, which is an interesting premise for future research.

As for the $LaBr_3(Ce)$ detector, due to its symmetrical photopeaks a single Gaussian peak shape model is adequate to fit photopeaks in a large energy range. ROI boundaries can be fixed at a level of *3σ* and *4σ* for the entire energy range.

The results of a performance assessment show that better energy resolution of a 500 mm^3 CZT detector does not provide any particular performance advantages over a 2 × 2 inch $LaBr_3(Ce)$ detector, apart from its compact size. Thus, due to the larger size of the latter it yields not only advantageous performance with the enrichment-meter method, but also the smallest uncertainties on the determined enrichment. Such behavior is dictated by the statistical quality of acquired spectra, which on a larger $LaBr_3(Ce)$ detector is better, despite its worse energy resolution compared to a 500 mm^3 CZT detector.

However, for those safeguards applications where detector size is a limiting factor, a 500 mm^3 CZT detector can be an attractive alternative. An interesting premise for future research in this domain would be a performance assessment of other sizes and designs of CZT detectors with the enrichment-meter method. Thus, as it was discussed in section 1, in recent years progress in CZT detector technologies has significantly improved their spectroscopic performance, both in terms of low-energy tailing effect and counting efficiency.

For similar acquisition times the difference in the net peak areas between the two detectors is about a factor of sixty. However, for a 500 mm^3 CZT detector net peak area uncertainties are noticeably larger

Table 11
2 × 2 inch $LaBr_3(Ce)$ results using CBNM446 as a calibration standard.

Declared enrichment, %	7200 s acquisition time							
	Three-window channel summation method				Function fit			
	Determined enrichment, %	Unc. ±	Rel. uncert., %	Bias, %	Determined enrichment, %	Unc. ±	Rel. uncert., %	Bias, %
2.95	2.95	0.006	0.22	0.15	2.97	0.04	1.34	0.68
1.95	1.96	0.005	0.27	0.51	1.93	0.03	1.48	−1.02
0.71	0.72	0.004	0.61	1.41	0.71	0.02	2.58	0.17
0.31	0.31	0.006	2.07	0.97	0.31	0.01	4.68	0.63

Table 12
500 mm^3 CZT results using CBNM446 as a calibration standard.

Declared enrichment, %	7200 s acquisition time							
	Three-window channel summation method				Function fit			
	Determined enrichment, %	Unc. ±	Rel. uncert., %	Bias, %	Determined enrichment, %	Unc. ±	Rel. uncert., %	Bias, %
2.95	2.95	0.06	2.01	0.10	2.84	0.23	8.02	−3.64
1.95	2.00	0.05	2.37	2.57	2.05	0.19	9.51	5.95
0.71	0.73	0.04	4.89	2.82	0.78	0.11	14.22	9.96
0.31	0.31	0.03	11.21	2.03	0.31	0.071	21.27	2.10

than those obtained for a 2 × 2 inch $LaBr_3$(Ce) detector, although the former has a better energy resolution. Such observed difference is due to the crystal size and related counting efficiency.

A natural continuation of our research work in the domain of room temperature medium resolution detectors application for uranium enrichment determination tasks is to further test them on a larger set of experimental uranium spectra counted through various absorbers and varying levels of background. Besides, opened question related to $LaBr_3$(Ce) detectors performance is the impact of internal activity of the ^{138}La radioisotope on the method performance and detection limits for measurement cases with low amounts of analyzing radioisotopes. Another interesting aspect would be to conduct an inter-comparison exercise between the traditional detectors (e.g. NaI and HPGe) performance used for uranium enrichment determination and the medium resolution ones (e.g. CZT and $LaBr_3$(Ce), including novel designs such as co-planar grid CZT and $LaBr_3$(Ce + Sr)) in terms of the accuracy and uncertainties achieved in different measurement conditions.

Declaration of competing interest

The authors declare that they have no known competing financial interests or personal relationships that could have appeared to influence the work reported in this paper.

Acknowledgements

This work was sponsored by Belgonucleaire NV and Tecnubel NV in the framework of the contract AC-2015-002 between SCK•CEN, Belgonucleaire NV and Tecnubel NV.

References

Arlt, R., Ivanov, V., Parnham, K., May 2000. Advantages and use of CdZnTe detectors in safeguards measurements. In: Presented at MPA&C Conference, Obninsk, Russia.
Arlt, R., Gunnink, R., 2001. Methods for evaluating and analyzing CdTe and CdZnTe spectra. Nucl. Instrum. Methods Phys. Res., Sec. A 458, 196–205, 2001.
Berndt, R., Mortreau, P., 2017. ^{235}U enrichment determination on UF_6 cylinders with CZT detectors. Nucl. Instrum. Methods Phys. Res. https://doi.org/10.1016/j.nima.2017.11.026.
Brown, A.M., 2001. A step-by-step guide to non-linear regression analysis of experimental data using a Microsoft Excel spreadsheet. Comput. Methods Progr. Biomed. 65, 191–200.
Carpenter, B.S., Gramlich, J.W., Greenberg, R.R., Machlan, L.A., DeBievre, P., Eschbach, H.L., Meyer, H., Van Audenhove, J., Connolly, V.E., Trahey, N.M., Zook, A.C., 1986. Uranium-235 Isotope Abundance Standard Reference Materials for Gamma Spectrometry Measurements. U.S. Department of Commerce, Malcolm Baldrige, Secretary National Bureau of Standards.
Fox, J., Weisberg, S., 2010. Nonlinear Regression and Nonlinear Least Squares in R: an Appendix to an R Companion to Applied Regression –, second ed.
Gunnink, R., Ruhter, W.D., Miller, P., Goerten, J., Swinhoe, M., Wagner, H., Verplacke, J., Bickel, M., Abousahl, S., 1994. MGA: a new analysis code for measuring U-235 enrichments in arbitrary samples,". In: IAEA Symposium on International Safeguards, Vienna, Austria, March 8-14, 1994. Lawrence Livermore National Laboratory (UCRL-JC-114713).
Gunnink, R., 2001. A Guide for Using NaIGEM Code, Version 1.5 for DOS and Windows.
Gilmore, G., 2008. Practical Gamma-Ray Spectrometry, second ed. John Wiley & Sons, Ltd, ISBN 978-0-470-86196-7.
Helmer, R.G., Lee, M.A., 1980. Analytical Functions for Fitting Peaks from Ge Semiconductor Detectors. Idaho National Engineering Laboratory, EG & G Idaho, Inc., Idaho Falls, Idaho 83415, USA.
Hu, W., Xie, J., Chau, H.W., 2015. Evaluation of parameter uncertainties in nonlinear regression using Microsoft Excel Spreadsheet. Environ. Sys. Res. 4 (4).
Ivanov, V., Dorogov, P., May 1999. Further development of hemispheric CZT detectors for safaguards applications. In: Proceedings of the 21st ESARDA Annual Symposium, Sevilla, Spain, pp. 4–6.
Ivanov, V., Mintcheva, J., Berlizov, A., Lebrun, A., 2014. Performance Evaluation of New Generation CdZnTe Detectors for Safeguards Applications.
Kull, L.A., Ginaven, R.O., 1974. Guidelines for Gamma-Ray Spectroscopy Measurements of ^{235}U Enrichment. Brookhaven National Laboratory report. BNL- 50414.
Maghraby, A.M., Alzimami, K.S., Alkhorayef, M.A., Alsafi, K.G., Mae, A., Alfuraih, A.A., Alghamdi, A.A., Spyrou, N.M., 2014. Investigation of $LaBr_3$:Ce probe for gamma-ray spectroscopy and dosimetry. Radiat. Phys. Chem. 95, 137–140.
Marquardt, D., 1963. An algorithm for least-squares estimation of nonlinear parameters. SIAM J. Appl. Math. 11, 431–441.
Matussek, P., 1985. "Accurate Determination of the ^{235}U Isotope Abundance by Gamma Spectrometry," A User's Manual for the Certified Reference Material EC-NRM-171/NBS-SRM-969. Karlsruhe, Germany.
Mcnelles, L.A., Campbell, J.L., 1975. Analytic Approximations to Peak Shapes Produced by Ge(Li) and Si(Li) Spectrometers. Department of Physics, University of Guelph, Guelph, Ontario, Canada.
Meleshenkovskii, I., Borella, A., Van der Meer, K., Bruggeman, M., Pauly, N., Labeau, P. E., Schillebeeckx, P., 2017a. Instrumentation effects on U and Pu CBNM standards spectra quality measured on a 500 mm^3 CdZnTe and a 2x2 inch $LaBr_3$(Ce) detectors. In: Proceedings of the ANIMMA 2017 Conference (Liege, Belgium).
Meleshenkovskii, I., Borella, A., Van der Meer, K., Bruggeman, M., Pauly, N., Labeau, P. E., Schillebeeckx, P., 2017b. Characterization of a 500 mm^3 CdZnTe detector for U and Pu isotopic composition determination tasks in safeguards. In: ESARDA Proceedings (Dusseldorf, Germany).
Meleshenkovskii, I., Pauly, N., Labeau, P.-E., 2018a. Determination of the uranium enrichment without calibration standards using a 2 × 2 inch LaBr3(Ce) room temperature detector and Monte Carlo sampling approach for uncertainty assessment. Eur. Phys. J. Plus 133 (12). https://doi.org/10.1140/epjp/i2018-12363-8.
Meleshenkovskii, I., Pauly, N., Labeau, P.-E., 2018b. Determination of the uranium enrichment without calibration standards using a 500 mm3 CdZnTe room temperature detector with a hybrid methodology based on peak ratios method and Monte Carlo counting efficiency simulations. Appl. Radiat. Isot. https://doi.org/10.1016/j.apradiso.2018.12.025.
Moré, J.J., 1977. The levenberg-marquardt algorithm: implementation and theory. In: Watson, G.A. (Ed.), Numerical Analysis. Springer Verlag, pp. 105–116. Lecture Notes in Mathematics 630.
Montero, M.P., Rubio, A., Martín Sánchez, A.M., 2004. Carrasco Lourtau, "Isotopic uranium and plutonium analysis by alpha-particle spectrometry. Nucl. Instrum. Methods Phys. Res. B 213, 429.
Nambooridi, M.N., Lavietes, A.D., McQuaid, J.H., 1996. Gamma-ray Peak Shape from Cadmium Zinc Telluride Detectors. Lawrence Livermore National Laboratory Report. UCRL-125271.
Parker, J.L., Reilly, T.D., 1972. The enrichment meter as a concentration meter. In: Robert Keepin, G. (Ed.), Nuclear Analysis Research and Development, Program Status Report, September-December 1972. Comp., Los Alamos Scientific Laboratory report, p. 11. LA-5 197-PR.
Prosper, E.I., Abebe, O.J., Ogri, U.J., 2012. Characterisation of cerium-doped lanthanum bromide scintillation detector. Lat. Am. J. Phys. Educ. 6.
Quarati, F.G.A., Khodyuk, I.V., Van Eijk, C.W.E., Quarati, P., Dorenbos, P., 2012. Study of 138La radioactive decays using LaBr3 scintillators. Nucl. Instrum. Methods Phys. Res. 683, 46–52.
Reilly, T.D., Walton, R.B., Parker, J.L., 1970. The enrichment meter – a simple method for measuring isotopic enrichment. In: Robert Keepin, G. (Ed.), Nuclear Safeguards Research and Development Program Status Report, September-December. Comp., Los Alamos Scientific Laboratory report LA-4605-MS, p. 19.
Reilly, D., Ensslin, N., Hastings Smith Jr., H., Kreiner, S., 1991. *Passive Nondestructive Assay of Nuclear Materials.* NuREG/CR-5550 LA-UR-90-732. Los Alamos National Laboratory, Los Alamos, NM.
Richter, S., Alonso, A., Truyens, J., Kühn, H., Verbruggen, A., Wellum, R., 2007. Evaluating the status of uranium isotope ratio measurements using an inter-laboratory comparison campaign. Int. J. Mass Spectrom. 264, 184.
Ritec Detectors Leaflet. http://www.ritec.lv/sdp500.html, 2019–. (Accessed 6 November 2019).
Routti, J.T., Prussin, S.G., 15 July 1969. Photopeak method for the computer analysis of gamma-ray spectra from semiconductor detectors. Nucl. Instrum. Methods 72 (Issue 2), 125–142.

Ruhter, W.D., 1998. Application of CZT detectors in nuclear materials safeguards. In: Proc. SPIE 3446, Hard X-Ray and Gamma-Ray Detector Physics and Applications, vol. 204.

Russell, J.T., June 1968. Method and Apparatus for Nondestructive Determination of ^{235}U in Uranium. US Patent No. 3389254.

Saint-Gobain detectors leaflet, 2019. https://www.crystals.saint-gobain.com/products/standard-and-enhanced-lanthanum-bromide. (Accessed 4 March 2019).

Sampson, T.E., Kelley, T.A., 1996. PC/FRAM: A Code for the Nondestructive Measurement of the Isotopic Composition of Actinides for Safeguards Applications. Los Alamos National Laboratory Report. LA-UR-96-3543.

Sato, G., Takahashi, T., Sugiho, M., Kouda, M., Mitani, T., Nakazawa, K., Okada, Y., Watanabe, S., 2002. Characterization of CdTe/CdZnTe detectors. IEEE Trans. Nucl. Sci. 49 (3), 1258–1263.

Simon, A.C., Espagnon, I., Pluquet, A., November . IGA (actinides gamma isotopy) an automatic software for the determination of actinides isotopic abundances. In: Presented at the International Workshop on Gamma Spectrometry Analysis Codes for U and Pu Isotopics, Oak Ridge, Tennessee.

Smith Jr., H.A., 1991. The measurement of uranium enrichment. In: Passive Non-destructive Assay of Nuclear Materials. (NUREG/CR-5550).

Sullivan, J.P., Rawool-Sullivan, M.W., Wenz, T.R., 2008. $LaCl_3$(Ce) and $LaBr_3$(Ce) gamma-ray spectra with various plutonium isotopic and uranium enrichment standards. J. Radioanal. Nucl. Chem. 276 (3), 699–705.

Takahashi, T., Watanabe, S., 2001. Recent progress in CdTe and CdZnTe detectors. IEEE Trans. Nucl. Sci. 48 (4), 950–959.

Van Loef, E.V.D., Dorenbos, P., Van Eijk, C.W.E., Kraemer, K.W., Guedel, H.U., 2001. High-energy-resolution scintillator: Ce^{3+} activated $LaBr_3$. Appl. Phys. Lett. 79, 1573.

Vo, D.T., April . Comparison of portable detectors for uranium enrichment measurements. In: Presented at the International Topical Conference Methods and Applications of Radioanalytical Chemistry – VII (MARC VII).

Walton, R.B., Reilly, T.D., Parker, J.L., Menzel, J.H., Marshall, E.D., Fields, L.W., 1974. Measurement of UF_6 cylinders with portable instruments. Nucl. Technol. 21, 133.